THE EFFECTS OF HIV-1 TRANSACTIVATOR OF TRANSCRIPTION (TAT) ON PRE-SYNAPTIC DENSITY IN THE TAT MOUSE MODEL OF HIV-1 ASSOCIATED NEUROCOGNITIVE DISORDER (HAND)

Megan Claudia Key

A thesis submitted to the faculty at the University of North Carolina at Chapel Hill in partial fulfillment of the requirements for the degree of Master of Science in the Neuroscience Curriculum at the School of Medicine

Chapel Hill
2020

Approved by:

Kelly S. Giovanello

Sylvia Fitting

Yen-Yu I. Shih

Graham H. Diering

Damaris N. Lorenzo

ABSTRACT

Megan Claudia Key: The effects of HIV-1 transactivator of transcription (Tat) on synaptic density in the Tat mouse model of HIV-1 associated neurocognitive disorder (HAND)
(Under the direction of Sylvia Fitting)

HIV-1 associated neurocognitive disorders (HAND) affect about 15-55% of HIV positive patients to date; and although the traditional form of therapy, combined antiretroviral therapy (cART), has been sufficient to suppress the more severe dementia-causing form of HAND, the proportion of seropositive patients experiencing minor neurocognitive disorders (MND) or asymptomatic neurocognitive impairments (ANI) due to HAND, has not changed. While cART therapy is inefficient in treating MND- and ANI-related HAND and its underlying synaptodendritic pruning pathology, cART does however decrease the occurrence of HIV-related encephalitis. This link neurocognitive decline to functional deficits in brain-wise microstructure and the characteristic degenerating synaptodendritic pruning morphology. HIV-1 neurotoxic transactivator of transcription (Tat) protein expression alone recapitulates this degenerative synaptic morphology and neuronal pathology. Thus, we utilized a Tat transgenic mouse model in this study to investigate the longitudinal effects of Tat on ubiquitous synaptic density *in vivo*. Positron-emission tomography (PET) imaging of the synaptic vesicle glycoprotein 2A (SV2A) selective radiotracer [^{11}C]-UCB-J, over three months, indicate a downregulation of SV2A in the frontal cortex of transgenic Tat(+) mice compared to Tat(−) controls over time. These findings suggest a decrease in synaptic density due to Tat expression, which might be a suitable biomarker for early disease progression in HIV-1 infection.

My Father in heaven, His miraculous power, thoughts, wisdom, and the best gift of His true Holy Spirit thanks to His Son Jesus Christ who was cursed for my complete deliverance!!

Perfect love

thank Jesus, the great mystery!!

Ephesians 1:9-11 NLT

https://www.bible.com/bible/116/eph.1.9-11.nlt

TABLE OF CONTENTS

LIST OF TABLES vii

LIST OF FIGURES viii

LIST OF ABBREVIATIONS ix

CHAPTER 1: INTRODUCTION 1

Human immunodeficiency virus type 1 (HIV-1)-associated neurocognitive disorder (HAND) 1

HIV-1 transactivator of transcription (Tat) 2

SV2A PET radiotracer [^{11}C]-UCB-J 3

Present experimental study 4

CHAPTER 2: MATERIALS AND METHODS 6

Animals 6

Positron emission tomography (PET) study 7

Radioligand synthesis of [^{11}C]-UCB-J *7*

Dynamic [^{11}C]-UCB-J PET imaging *7*

PET image analysis *9*

Statistical analysis 10

CHAPTER 3: RESULTS 11

Time-activity SUV curves of [^{11}C]-UCB-J PET over a 60 minute time period 11

SUV for brain/muscle ratio at the static 17.5 minute time point 11

SUV for brain/muscle ratio at the static 25 minute time point 12

SUV for brain/muscle ratio averaged across the static 17.5 and 25 minute time points 13

CHAPTER 4: DISCUSSION 15

HIV-1 associated neurocognitive disorder (HAND) post-cART – Overview 15

Viral toxins 15

Transactivator of Transcription (Tat) and glycoprotein (gp120) *16*

CHAPTER 5: CONCLUSION 18

TABLES 20

FIGURES 21

REFERENCES 27

LIST OF TABLES

Table 1. Age, body weight and injection dose by genotype in Tat transgenic mice..... 20

LIST OF FIGURES

Figure 1. Scheme showing the experimental design of the conducted study on timeline 21

Figure 2. Time-activity SUV curves of [^{11}C]-UCB-J PET over a 60 minute time period..... 22

Figure 3. Decreased [^{11}C]-UCB-J binding in a Tat(+) mouse compared to a Tat(−) mouse..... 23

Figure 4. SUV brain/muscle ratio normalized to baseline (% change) at the static 17.5 minute time point 24

Figure 5. SUV brain/muscle ratio normalized to baseline (% change) at the static 25 minute time point 25

Figure 6. SUV brain/muscle ratio normalized to baseline (% change) and averaged across the static 17.5 and 25 minute time points 26

LIST OF ABBREVIATIONS

AIDS	acquired immunodeficiency syndrome
ANOVA	analysis of variance
ANI	asymptomatic neurocognitive impairment
BW	body weight
cART	combined antiretroviral therapy
CNS	central nervous system
CT	computed tomography
DOX	doxycycline
GABA	gamma aminobutyric acid
GFAP	glial fibrillary acidic protein
HIV-1	human immunodeficiency virus type-1
HAD	HIV-associated dementia
HAND	HIV-1 associated neurocognitive disorders
ID	injection dose
mIPSC	miniature inhibitory post-synaptic current
MND	minor neurocognitive disorder
MRI	magnetic resonance imaging
neuroHIV	neuro- human immunodeficiency virus
OSEM	ordered subject expectation maximization
PET	positron emission tomography
SD	standard deviation of the mean
SUV	standard uptake value

SV2A	synaptic vesicle glycoprotein 2A
S1	session 1
S2	session 2
S3	session 3
Tat	transactivator of transcription

CHAPTER 1: INTRODUCTION

Human immunodeficiency virus type 1 (HIV-1)-associated neurocognitive disorder (HAND)

The World Health Organization estimates 36.7 million people are diagnosed with human immunodeficiency virus type 1 (HIV-1) worldwide, which has been considered a fatal diagnosis before antiretroviral treatments were established. With the introduction of combined antiretroviral therapy (cART), HIV-1 infection has changed from a death sentence to a manageable condition with decreased mortality rates and increased life expectancies[1-3]. For example, the development and treatment of HIV-1 with cART has decreased the prevalence of acquired immunodeficiency syndrome (AIDS)-related deaths by 50%[2]. However, as cART is not able to eradicate the effects on the central nervous system (CNS), HIV-1 is now considered a chronic disease that specifically targets the brain with at least 15-55 office seropositive individuals experiencing some form of HIV-1-associated neurocognitive disorders (HAND)[4-7]. HAND consists of three subtypes: the more severe HIV-associated dementia (HAD), minor neurocognitive disorder (MND), and asymptomatic Neuro cognitive impairment (ANI)[2]. cART treatment has significantly decreased the incidence of the more severe form of HAND, HAD, by 40-50%, but the milder forms, MND or ANI, remain the same in the post-cART era[3-7], indicating cART's therapeutic inefficiency against HAND, especially for the milder forms. Not only this, but cART treatment also accelerates toxicity and dysfunction over long-term use[8].

The severity of the pathophysiology underlying MND and ANI are thought to be more associated with functional neurological changes rather than encephalitis, including increased subtle changes in gray matter volume as well as supporting white matter microstructures that become apparent with age, marking depressed synaptic communication[9]. Additionally, post-mortem tissue analyses on HIV-1 infected patients with MND and ANI indicate specific effects on synaptic connectivity, including dendritic beading, synaptic degeneration, dendritic spine loss, and axonal disruption; all important machineries for cell communication, neurological function, and cognition[10]. HIV-1 contributes to these observed neuronal deficits through the continued production of neurotoxic HIV-1 proteins, including the transactivator of transcription (Tat). Tat is released from cellular reservoirs within the CNS of cART-treated HIV patients[11]. Importantly, cART treatment seems to have little or no effect on the secretion rate of Tat from infected cells in the CNS as Tat remains present in the blood of HIV-1 patients, extending viral replication and HAND pathology[11,12].

HIV-1 transactivator of transcription (Tat)

Tat is a regulatory protein within the genome of HIV-1 that drastically enhances the efficiency of viral transcription, hence the name "Trans-Activator of Transcription" (Tat). Although Tat is not produced within neurons, it is one of the first toxic proteins expressed from macrophages and glial cells after HIV-1 infection occurs and is a contributor to the synaptodendritic injury observed in HIV-1 infected individuals[2,13,14]. Tat has been shown to cause structural and functional neuronal defects *in vitro*[15-18] and *in vivo*[19-23]. For example, Tat has been shown to stimulate neurons, cause increases in $[Ca^{2+}]_i$, overproduction of free radicals, and disruption of neurotransmitter homeostasis, all of which likely leads to synaptodendritic

injury[18,24-27]. The expression of Tat in transgenic mice also recapitulates axonal and synaptic degeneration similar to that observed in cART-treated patients with MND and ANI[19]. Expression of Tat in these transgenic mice demonstrated to significantly reduce motor cortical thickness as well as axonal and synaptic vesicle proteins, respectively: the neuronal microtubule marker βIII-Tubulin, presynaptic vesicle protein synaptophysin, and postsynaptic density 95 (PSD-95) protein; all associated with synaptodendritic injury caused by Tat expression [28]. Nevertheless, it is unknown how Tat is targeted at the pre-synapse to produce these pathological changes, which is the focus of the present study.

SV2A PET radiotracer [^{11}C]-UCB-J

Synaptic vesicle glycoprotein 2A (SV2A) is a 12-transmembrane protein found within synaptic vesicles in neurons and in endocrine cells of the peripheral nervous system[29]. It is one of three isoforms, SV2A, SV2B, and SV2C all of which are expressed within different regions of the brain[30]. The function and mechanism of SV2A is not well understood; however, the membrane bound protein has been implicated in epilepsy and neuro-cognition via its critical role in ubiquitous neurotransmission[31]. Lack of SV2A results in seizures and death marking its necessity for life and neuro-communication or transmission[32]. SV2A has also been shown to be a good biomarker of pre-synaptic density and neurocognitive impairment or injury.

Because of the importance of the SV2A involved in many neurological diseases, non-invasive imaging techniques to monitor and quantify the level of SV2A using have been developed in recent years. PET imaging has been chosen as the most effective tool due to its high sensitivity capable to detect in pico-molar concentration changes. Several PET tracers such as the SV2A ligands have been developed since 2015. Among them, [^{11}C]-UCB-J has been identified as the

most promising probe with high affinity and sufficient penetration to the blood-brain-barrier. It was first reported and evaluated in rhesus macaque model[29]. [^{11}C]-UCB-J biodistribution study demonstrated high uptake in all grey matter regions with fast kinetics, and blocking study also demonstrated its high specificity as a SV2A ligand[29]. Recently [^{11}C]-UCB-J PET imaging has been evaluated in human subjects[29] and rodent models[33,34]. Significant hippocampal reductions in [^{11}C]-UCB-J correlated with mild neurocognitive impairment and dementia in Alzheimer's patients[35] to demonstrate the ligand's proficiency as a global pre-synaptic marker for injury. Further, the downregulation of synaptic density in the hippocampus via [^{11}C]-UCB-J was also demonstrated in a preclinical mouse model of Alzheimer's disease[34]. Therefore, PET analysis with the SV2A-brain-specific [^{11}C]-UCB-J radioligand can provide a more thorough analysis of pre-synaptic density in the HAND-related Tat transgenic mouse model for future understanding of its mechanism of pathology. [^{11}C]-UCB-J is also one of the first radioligands for a presynaptic marker, and therefore makes it distinct for dementia related diseases such as HAND[36], Alzheimer's disease, and even neuropsychiatric diseases [36].

Present experimental study

Loss of neuronal synaptic structure has been mostly reported within the excitatory nervous system of HAND studies, with more emphasis on a post-synaptic mechanism of Tat's neurotoxic effects; however, there is limited understanding on HIV-1 Tat's effect on global neuronal pre-synapses. Recent electrophysiology findings from our laboratory established Tat as a significant effector of GABAergic miniature inhibitory post-synaptic current (mIPSC) frequencies in the prefrontal cortex of Tat transgenic mice (manuscript currently under review). This decreasing effect on GABAergic mIPSC frequencies supports the idea for a negative Tat

effect on inhibitory pre-synaptic vesicular release. A previously published study further validates a pre-synaptic effect of HIV-1 Tat via a significant decrease in the pre-synaptic synaptotagmin II expression levels[19]. Notably, expression of synaptotagmin I at the pre-synapse is also critically dependent on the expression and co-trafficking of the synaptic vesicle glycoprotein SV2A, which is a brain-specific ubiquitous pre-synaptic vesicle membrane bound protein, and found at excitatory and inhibitory synapses critical for neurotransmission[37]. SV2A is critical for synaptic function as it is expressed ubiquitously in pre-synaptic secretory vesicles in all brain areas and its dysfunction has been implicated in epilepsy and Alzheimer's disease[38,39]. With the recent development of the SV2A PET radiotracer [^{11}C]-UCB-J, it has now been possible to measure synaptic density in humans, nonhuman primates, and rodents *in vivo*[29,34,40]. The use of the [^{11}C]-UCB-J ligand in our Tat transgenic mouse modeling HAND will therefore provide longitudinal information about changes in synaptic density with Tat expression. In the present study, I hypothesize that HIV-1 Tat disrupts synaptic density depending on exposure time, resulting in a downregulation of SV2A with chronic Tat exposure and therefore, a decrease in [^{11}C]-UCB-J uptake. Understanding the exact mechanisms of Tat's effect on the synapse can yield new targets for more efficient treatment against Tat related detrimental effects on the CNS and potentially HAND.

CHAPTER 2: MATERIALS AND METHODS

Animals

HIV-1 Tat_{1-86} transgenic mice were used in the present study and developed on a C57BL/6J hybrid background. In this HIV-1 Tat transgenic mouse line HIV-1 Tat_{1-86} is expressed in astrocytes in a brain-specific, doxycycline (DOX) inducible manner[41,42]. The Tat transgenic mice are a well-established model for HAND since their neuropathology tends to mirror those observed in treated HIV+ patients with HAND , including structural abnormalities[20,41], disrupted hippocampal circuitry[19], as well as glial abnormalities[41,42]. Importantly, these mice and a related Tat transgenic mouse model develops changes in learning and memory relevant for HIV-1 patients[19,21,41,43-45]. Thus, chronic low level of Tat expression in this animal model is a good simulator of virally-suppressed, post-cART era HIV-1 treated patients, neurological damage, and the synaptodendritic decline experienced[19,28].

In the present study longitudinal PET imaging with [^{11}C]-UCB-J was conducted on Tat(+) and control Tat(−) mice (n = 6 (3f)/per group) at three time points (mean ± SD): baseline [prior to Tat induction; session 1 (S1)], 2 weeks post Tat induction [bvfbjnbC session 2 (S2)], and 3 months post Tat induction [session 3 (S3)]. In the female Tat(+) group one subject had to be excluded due to head movement artifacts during the 60 minutes of PET imaging. The demographics are summarized in **Table 1**. For baseline imaging, mice received normal chow (IsoPro RMH 3000, Purina LabDiet, St Louis, MO) and water available *ad libitum* before Tat induction to assess baseline SV2A expression. After baseline imaging, animals were fed a specially formulated chow containing 6 mg/g DOX (Harlan, Indianapolis, IN, product #:

TD.09282) to induce Tat expression in mice that express the *GFAP-rtTA* and *TRE-tat* genes [Tat(+) mice]. Control Tat(−) transgenic mice that express only the *GFAP-rtTA* gene and lack the *tat* transgene received the same DOX diet after baseline PET imaging was conducted. Previous studies have shown increased astrocyte activation and elevations in caspase-3 as well as elevated tissue levels of CCL5/RANTES and IL-6 after only 2-day DOX exposure in Tat(+) mice compared to Tat(−) mice[42,46]. Mice had free access to water and DOX food during the entire experimental study and were group housed (2-4 mice per cage) on a reversed 12 h light/dark cycle (lights on at 8:00 AM). All animal procedures were approved by the University of North Carolina Institutional Animal Care and Use Committee (IACUC) and are in keeping with ethical guidelines defined by the National Institutes of Health (NIH Publication No. 85-23).

Positron emission tomography (PET) study

Radioligand synthesis of [^{11}C]-UCB-J

The synthesis of [^{11}C]-UCB-J was performed as previously described[29]. The [^{11}C]-UCB-J probe was produced at the Biomedical Research Imaging Center Cyclotron and Radiochemistry Core facility according to the well-established radiosynthesis method[29]. Radiochemical purity was > 99% and the specific activity was 463.61 ± 108.78 GBq/μmol.

Dynamic [^{11}C]-UCB-J PET imaging

All animal PET imaging paired with computed tomography (CT) scanning were performed during the daylight cycle and conducted in the Small Animal Imaging facility of the Biomedical Research Imaging Center at three time points: baseline prior Tat induction (S1), 2 weeks post Tat induction (S2), 3 months post Tat induction (S3). PET/CT image acquisition was

performed using a small animal PET/CT scanner (SuperArgus, Sedecal Molecular Imaging, Inc. Spain) with a spatial resolution of 1.0 mm in the center field of view using 3D-ordered subject expectation maximization (3D-OSEM) reconstruction algorithm. The SuperArgus PET/CT system is equipped with the depth-of-interaction correction technique resulting in the reduction of resolution degradation along the trans-radial direction[47], so that multi-animal imaging can be conducted with less radial distortion at the edge of the bore.

Animals were anesthetized with inhalation of 1.5%-2.5% isoflurane-oxygen gas mixture. A tail vein catheter with 30 g needle was placed for each animal for the injection of radiotracer. The 12 mice were divided into 3 batches with 4 mice per batch (including both genotypes and both sexes per session). For each PET imaging, four mice were placed on a 4-bed mouse holder and securely attached to the nose cone supplied with 1.5-2.5% isoflurane-oxygen mixture. Respiration probe were placed near the chest of each mouse to monitor respiration rate, and a rectal temperature probe was placed to measure body temperature. A dose of [^{11}C]-UCB-J (350 - 450 μCi in 150 μL saline) was administered through mouse tail vein. Simultaneously, a 60 minute dynamic PET scan was acquired in list mode with energy window of 350-700 keV. After PET acquisition, a CT scan was conducted to obtain anatomical structure and attenuation correction. Anesthesia was maintained throughout the imaging and body temperature was maintained using a heat lamp. Mice were recovered from anesthesia after imaging and returned back to the housing facility. A repeated PET/CT imaging was conducted at 2 weeks and 3 months post Tat induction. The information of imaging animals at the three time points are summarized in **Table 1**.

Following image acquisition, the raw dynamic PET data were binned into 19 time frames (6x10 s, 4x30 s, 2x60 s, 3x300 s, 4x600 s), and images were reconstructed using 3D-OSEM

algorithm (25 OSEM iterations) with corrections for scatter, random, decay, and attenuation. The resulting PET images were in 0.370x0.370x0.775 mm voxel size, and 120 mm axial field of view. Standardized uptake value (SUV) was calculated voxel-wise based on the injection dose (ID) and animal body weight (BW) with the formula: SUV=S/ID*BW (S is the radioactivity level per voxel). Standard T2-weighted magnetic resonance images were acquired from eight Tat transgenic mice to form an averaged magnetic resonance imaging (MRI) atlas and provide the substructure reference within brain for the PET images.

PET image analysis

PET analysis was performed using PMOD 4.0 version (PMOD Technologies LLC, Switzerland). PET images were first registered to the MRI atlas images via co-registered CT images. Once co-registration was complete, the cerebrum was drawn in the MRI images as the volume of interest and superimposed to PET images to extract the time-activity curves of cerebrum from 19 time frames over 60 minutes. Similarly, SUVs were calculated for heart, liver and muscle. To assess group differences in the SUVs, the SUV of cerebrum was normalized to the SUV of muscle. The muscle uptake is used as a self-control to reduce the inter-subject errors in measuring injection doses and differences in plasma distributions. The brain to muscle ratios at the 17.5 and 25 minute time points when the uptake in brain reached plateau were compared among baseline, 2 weeks, and 3 months post Tat induction. Data are graphed as percentage change at 2 weeks and 3 months post induction to the baseline level.

Statistical analysis

Data were analyzed by mixed-model analysis of variance (ANOVA) with time as a within-subjects factor (3 levels: S1, S2, S3), and genotype [2 levels: Tat(−), Tat(+)] and sex (2 levels: males, females) as between-subjects factors followed by Bonferroni post hoc tests when appropriate (SPSS Statistics 25; IBM, Chicago, IL). Analyses were followed up with paired-samples *t*-tests for significant interactions between time and genotype and/or sex. Differences of p-values ≤ 0.05 were considered statistically significant. All data are presented as mean ± the standard deviation of the mean (SD).

CHAPTER 3: RESULTS

Time-activity SUV curves of [^{11}C]-UCB-J PET over a year 60 minute time period

Average time-activity SUV curves of [^{11}C]-UCB-J PET for each of the three sessions are presented separately for each genotype in **Figure 2.** SUVs for the cerebrum and muscle are shown separately. The time-activity SUV curves in the cerebrum for Tat(−) mice (**Figure 2A**) compared to Tat(+) mice (9 **Figure 2B**) show higher variability and less separation between sessions. For both genotypes the time-activity SUV curves show high [^{11}C]-UCB-J ligand uptake in the cerebrum and low uptake in the muscle. No appreciable difference in the distribution or washout of the [^{11}C]-UCB-J ligand is seen in the cerebrum or muscle for either genotype. Representative overlay images of a Tat(−) mouse and a Tat(+) mouse are presented in **Figure 3**.

SUV for brain/muscle ratio at the static 17.5 minute time point

Results of the SUV for brain/muscle ratio at 17.5 minutes PET scan are summarized in **Figure 4**. A three-way mixed ANOVA revealed a significant main effect for time, F (2, 14) = 8.95, p = .003, with a significant overall downregulation of SUV over PET sessions (S1 vs. S3: n = 11, p = .026; S2 vs. S3: n = 11, p = .049). The p-value of .026, infers that SV2A is overall decreased after 3 months of DOX treatment (S3) compared to baseline, when animals did not receive DOX treatment (S1). Further the p-value of .049 indicates that there was also a significant decrease seen after 3 months of DOX treatment (S3) compared to 2 weeks of DOX treatment (S2). More importantly however, this main effect of time is significantly altered by

genotype, indicated by a significant interaction between time and genotype, F (2, 14) = 3.91, p = .045, suggesting that DOX chow treatment, significantly alters [^{11}C]-UCB-J uptake depending on whether DOX induces Tat expression [Tat(+) mice] or not [Tat(−) mice] (**Figure 4A**). Paired-samples *t*-tests within each genotype demonstrate that the significant downregulation of SUV over time was only found with Tat expression in Tat(+) mice for baseline assessments prior Tat induction (S1) compared to 3 months post Tat induction (S3; n = 5, t(4) = 3.28, p = .031) and for assessments at 2 weeks post Tat induction (S2) compared to 3 months post Tat induction (S3; n = 5, t(4) = 3.14, p = .035). In contrast, no significant differences were noted for Tat(−) mice between any time points. No other effect and/or interaction was significant, indicating that sex does not alter the brain/muscle ratio at the static 17.5 minute time point (**Figure 4B-C**). Overall, the findings suggest that [^{11}C]-UCB-J uptake is decreased in Tat(+) mice compared to Tat(−) mice due to Tat induction significantly downregulating SV2A expression in the vesicles or pre-synapses. Hence, pre-synaptic vesicles significantly decrease with Tat induction in Tat(+) mice when assessed in a longitudinal study, compared to Tat(−) mice that do not express the Tat protein.

SUV for brain/muscle ratio at the static 25 minute time point

Results of the SUV for brain/muscle ratio at 25 minutes PET scan are summarized in **Figure 5**. A three-way mixed ANOVA revealed a significant main effect for time, F (2, 14) = 8.57, p = .004, with a significant overall downregulation of SUV over PET sessions (S1 vs. S3: n = 11, p = .009). Importantly, there is a significant interaction between time and genotype, F (2, 14) = 3.66, p = .053, with decreased SV2A uptake seen in Tat(+) mice but not Tat(−) mice (**Figure 5A**). Paired-samples *t*-tests within each genotype demonstrate a significant

downregulation of SV2A uptake in Tat(+) mice for baseline assessments prior Tat induction (S1) compared to 3 months post Tat induction (S3; $n = 5$, $t(4) = 3.58$, $p = .023$). In contrast, no significant differences were noted for Tat(−) mice between any time points. No other effect and/or interaction was significant, indicating that sex does not alter the brain/muscle ratio at the static 25 minute time point (**Figure 5B-C**). Thus, similar to the findings at 17.5 minutes, [^{11}C]-UCB-J uptake is decreased in Tat(+) mice compared to Tat(−) mice, which however was only noted between the first baseline PET session (S1) and the last session when Tat was induced for 3 months (S3).

SUV for brain/muscle ratio averaged across the static 17.5 and 25 minute time points

Results of the SUV for brain/muscle ratio averaged across the two static 17.5 and 25 minute time points are summarized in **Figure 6**. A three-way mixed ANOVA revealed a significant main effect for time, $F(2, 14) = 9.70$, $p = .002$, with a significant overall downregulation of SUV over PET sessions (S1 vs. S3: $n = 11$, $p = .012$). Importantly, there is a significant interaction between time and genotype, $F(2, 14) = 4.21$, $p = .037$, with decreased SV2A uptake seen in Tat(+) mice but not Tat(−) mice (**Figure 6A**). Paired-samples *t*-tests within each genotype demonstrate a significant downregulation of SV2A uptake in Tat(+) mice for baseline assessments prior Tat induction (S1) compared to 3 months post Tat induction (S3; $n = 5$, $t(4) = 3.53$, $p = .024$) and for assessments at 2 weeks post Tat induction (S2) compared to 3 months post Tat induction (S3; $n = 5$, $t(4) = 2.78$, $p = .050$). In contrast, no significant differences were noted for Tat(−) mice between any time points. No other effect and/or interaction was significant, indicating that sex does not alter the brain/muscle ratio for the two time point averages (**Figure 6B-C**). Thus, these findings indicate that the uptake of the [^{11}C]-

UCB-J ligand over an 8 minute time period follows the trend demonstrated at the static 17.5 minute time point, with a significant downregulation of SV2A expression between the first PET session at baseline (S1) and 3 months of Tat induction (S3), as well as between 2 weeks of Tat induction (S2) and S3.

CHAPTER 4: DISCUSSION

HIV-1 associated neurocognitive disorder (HAND) post-cART – Overview

Synapses are important for the function of the brain. In HIV-1 associated neurocognitive disorders (HAND), synapses are decreased partly due to the toxins released by the immune system in the brain and an over-excited or imbalanced neuronal system. Such toxins such as gp120, Nef, and Tat are released in different ways from the virus, either via microglia, macrophages, and astrocytes that are actively and inactively infected by HIV-1[48]. While neurons are not directly infected, they undergo degeneration due to such toxins and excitotoxicity by mechanisms only partly known or acknowledged.

Prior to cART therapy HIV-1 with encephalitis (HIVE) resulting from increased inflammation due to the infection of glial and the white blood cells previously mentioned, made up a larger amount of the HAND cases along with the most severe form, HAD. However, with cART treatment these forms of HAND have decreased and the less severe form MND, persist with less occurrences of encephalitis; meaning, the disease within these less severe cases is due to the degeneration of neurons, white matter connections, or other co-morbidities as HIV-1 is a highly co-morbid disease[49].

Viral toxins

Accumulation of HIV-1 toxins leads to the damage of neurons and the breakdown of

such synapses in the neurodegenerative HAND and similar dementia-associated diseases such as Alzheimer's disease and psychiatric disorders. In the post-cART era HIV-1 rests more latently in the brain as patients treated for the virus have undetectable serum levels. cART's inefficiency to treat the virus in the CNS and it's harsh medicinal effects contribute to HAND and compound toxicity[50]. There are several other toxins from the virus that result in disease morphology in HAND: the envelope glycoproteins gp120, gp160 and gp41, the non-structural proteins Nef, the trans-activating gene and regulatory protein Tat which also regulates viral replication Rev, and another HIV-1 accessory protein vpr[51]. These toxins are most likely found within macrophages and microglial cells in MND and ANI HAND patients as these cells harbor latent virus with suppressive cART treatment[52]. The astrocytes role as a viral reservoir or toxin store for degradation and release, is one up for debate[53].

Transactivator of Transcription (Tat) and glycoprotein (gp120)

Two of these toxins are popularly investigated in HAND systemically within the post-cART era - gp120 and Trans-activator of transcription Tat. Tat and gp120 both target and effect separate components of brain cell biology to produce HAND, the immune related cells and vasculature for the former and major brain functioning neurons and astrocytes for the latter. Even though gp120 is toxic to endothelial cells of the BBB and is necessary to initiation of viral entry into the CNS especially in HIVE, it is found at higher levels within the serum rather than the CNS and has less effect in HAND without encephalitis[54,55]. Therefore, the toxic contributions of gp120 may occur early on to be masked by glutamate and Tat as its detection in HIV autopsy brains is low[55].

Tat targets both neurons and astrocytes post secretion from infected macrophages and microglia within the Tat transgenic mouse model to cause disease pathology[28,56]. In astrocytes this includes, glial I brillar y acidic protein (GFAP) aggregation, lysosomal exocytosis, and glutamate excitotoxicity which contribute to neuronal cell death in HAND[57].Tat produces similar effects in neurons altering GABA and glutamate neurotransmitter release with opposite effects on each; increasing glutamate via AMPA and acetylcholine receptors and decreasing GABA neurotransmitter release [58]. The inhibition of neurotransmitter release was investigated in relation to the inositol 1,4,5 -triphosphate (IP3) pathway.

CHAPTER 5: CONCLUSION

Accumulated Tat in the extra-cellular space is believed to increase intercellular calcium levels to dysregulate its influx and eventually lead to increased exocytosis of neurotransmitters and glutamate excitotoxicity. Increased membrane depolarization is initially mediated through the IP3 pathway which fuels the over activation and stress of neurons and astrocytes seen in the HAND phenotype [26,59] .Using chromaffin and PC12 neuroendocrine cells it was shown that Tat is trafficked intracellularly via endosomes to bind and sequester IP3, and eventually inhibit neurosecretion and associated proteins such as annexin A2 which promotes lipid microderm formation [60] .

This study along with several others linked Tat to the endo- and exo-cytosis pathway within the periphery. This however, has not been shown within the CNS; but, a study analyzed Tat's effect within neurons to show it increases mir-128 to inhibit vesicular proteins like SNAP-25, a pre-synaptic protein, and SV2A the ubiquitous glycoprotein found within pre-synapses[61] . This also verifies Tat's pre-synaptic effects on neurons and its association to SV2A which corresponds with the negative Tat effect we show on 11C-UCB-J uptake and the ubiquitous pre-synaptic density.

Due to low n numbers and variability with the imaging process, we cannot conclude with great certainty that Tat significantly decreases SV2A expression as we still need to conduct dynamic analysis and kinetic modeling to analyze longitudinal effects of Tat on 11C-UCB-J and hence pre-synapses; but our data indicate that Tat depreciates 11C-UCB-J's target.

How and if Tat alters 11C-UCB-AJ's bonding to SV2A is not analyzed, but an SV2A blocker or different sized Tat proteins could be used to see whether Tat interacts with SV2A and what portion of the protein is important for these effects would be a good study to examine this. Also, analysis of Tat's effect ex vivo via western blot or immunohistochemistry would be a good follow up for verification. A recent study shows that CBD or epidiolex interacts with SV2A and would make a good blocker or drug to analyze. I propose that Tat interacts with SV2A and synaptotagmin as its mechanism of internalization through endocytosis to alter the endo-exocytosis pathway (not shown).

TABLES

Table 1. Age, body weight and injection dose by genotype in Tat transgenic mice

	Parameter/ Session	Age (days)	Age (months)	Body Weight (gram)	Injection dose (μCi)
Tat (-)	Baseline	95.8±4.22	3.2±0.14	25.2±3.53	404.0±26.43
n = 6 (3f)	2 weeks	112.8±1.17	3.8±0.04	25.9±3.55	323.9±69.27
	3 months	181.8±1.17	6.1±0.04	30.4±2.18	324.1±40.51
Tat (+)	Baseline	96.6±3.13	3.2±0.10	26.2±3.46	383.0±46.50
n = 5 (2f)	2 weeks	112.6±0.55	3.8±0.02	27.6±3.34	330.0±100.22
	3 months	181.6±0.55	6.1±0.02	30.4±3.68	337.7±35.35

Data are mean ± SD.

FIGURES

Figure 1. Scheme showing the experimental design of the conducted study on timeline

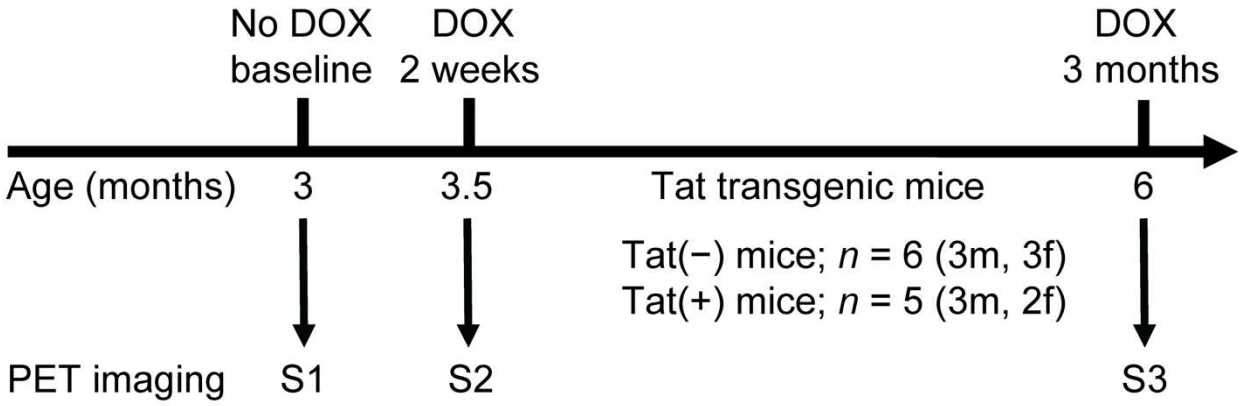

Figure 1. At 3 months of age Tat transgenic mice (*n* = 5-6 per group/3 males, 2-3 females) were PET imaged without having received DOX treatment (S1, baseline). Following PET imaging Tat transgenic mice were put on DOX treatment and PET imaged again after 2 weeks of DOX exposure (S2, 2 weeks DOX). The last PET imaging session as conducted after 3 months of DOX exposure (S3). m: male, f: female; S1: session 1; S2: session 2; S3: session 3.

Figure 2. Time-activity SUV curves of [^{11}C]-UCB-J PET over a 60 minute time period

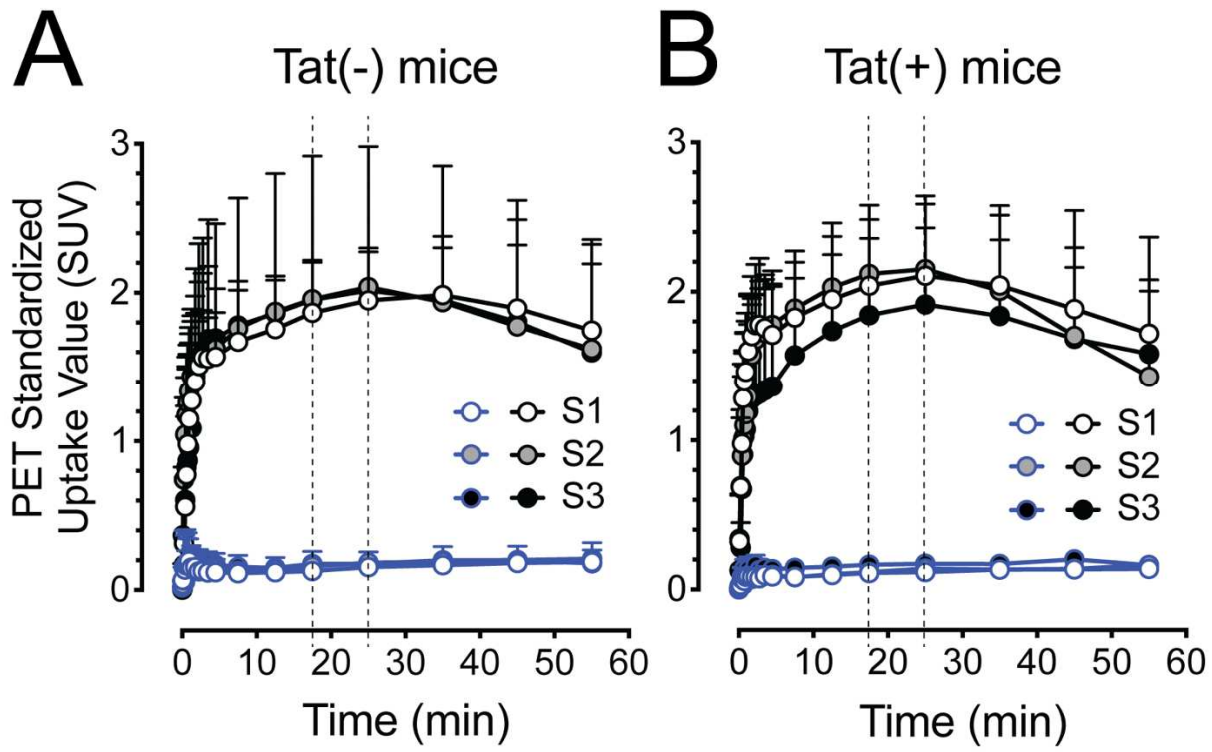

Figure 2. Average time-activity curves of [^{11}C]-UCB-J PET representingi the standardized uptake value (SUV) for the cerebrum (black lines) and muscle (blue lines) over a 60 minute time period separately for **(A)** Tat(−) mice and **(B)** Tat(+) mice. All data are presented as mean ± SD (*n* = 5-6 per group). S1: session 1; S2: session 2; S3: session 3.

Figure 3. Decreased [^{11}C]-UCB-J binding in a Tat(+) mouse compared to a Tat(−) mouse

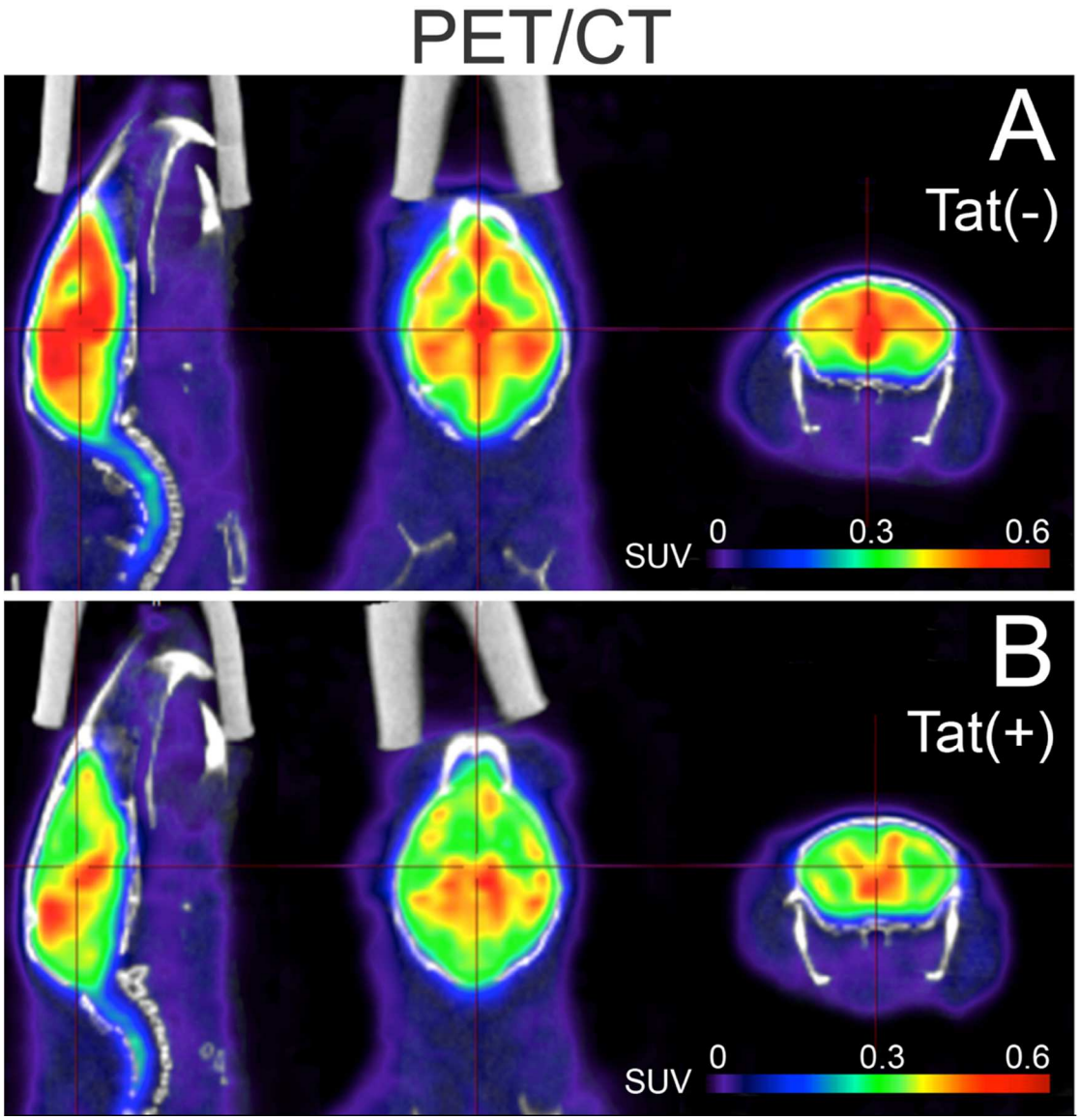

Figure 3. Representative overlay images of a Tat(−) mouse and a Tat(+) mouse show CT imaging (white) and PET imaging using the synaptic vesicle glycoprotein 2A (SV2A) selective radiotracer, [^{11}C]-UCB-J (SUV scale, yellow-red). Both mice have been exposed to DOX for 3 months. The Tat(+) mouse indicates a downregulation of [^{11}C]-UCB-J uptake in the brain compared to the Tat(−) mouse, suggesting Tat expression decreases synaptic density. PET: positron emission tomography; CT: computed tomography; SUV: standard uptake value; DOX: doxycycline.

Figure 4. SUV brain/muscle ratio normalized to baseline (% change) at the static 17.5 minute time point

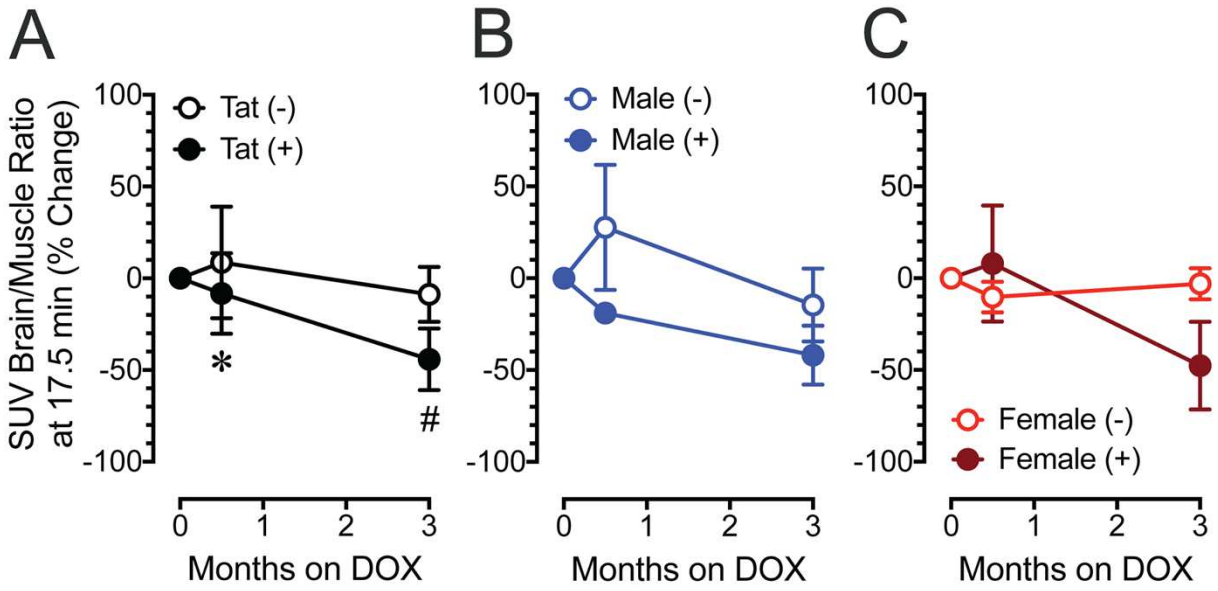

Figure 4. SUV for brain/muscle ratio normalized to baseline (% change) at 17.5 minutes. **(A)** SUV brain/muscle ratio of [^{11}C]-UCB-J uptake is represented over the three PET imaging sessions separate for Tat(−) and Tat(+) mice (n = 5-6 per group). A significant time x genotype interaction demonstrates a downregulation of SUV brain/muscle ratio over time for Tat(+) mice but not for Tat(−) mice. No other effect and/or interaction was significant, indicating that sex does not alter the SUV brain/muscle ratio at the static 17.5 minute time point. **(B)** SUV brain/muscle ratio of [^{11}C]-UCB-J uptake is represented over the three PET imaging sessions separate for males only (n = 3 per group). No significant effect for genotype and/or time was noted. **(C)** SUV brain/muscle ratio of [^{11}C]-UCB-J uptake is represented over the three PET imaging sessions separate for females only (n = 2-3 per group). No significant effect for genotype and/or time was noted. All data are presented as mean ± SD. $^{\#}p$ = 0.031 Tat(+) at baseline no DOX (S1) vs. Tat(+) at 3 months DOX (S3); $*p$ = 0.035 Tat(+) at 2 weeks DOX (S2) vs. Tat(+) at 3 months DOX (S3). min: minutes.

Figure 5. SUV brain/muscle ratio normalized to baseline (% change) at the static 25 minute time point

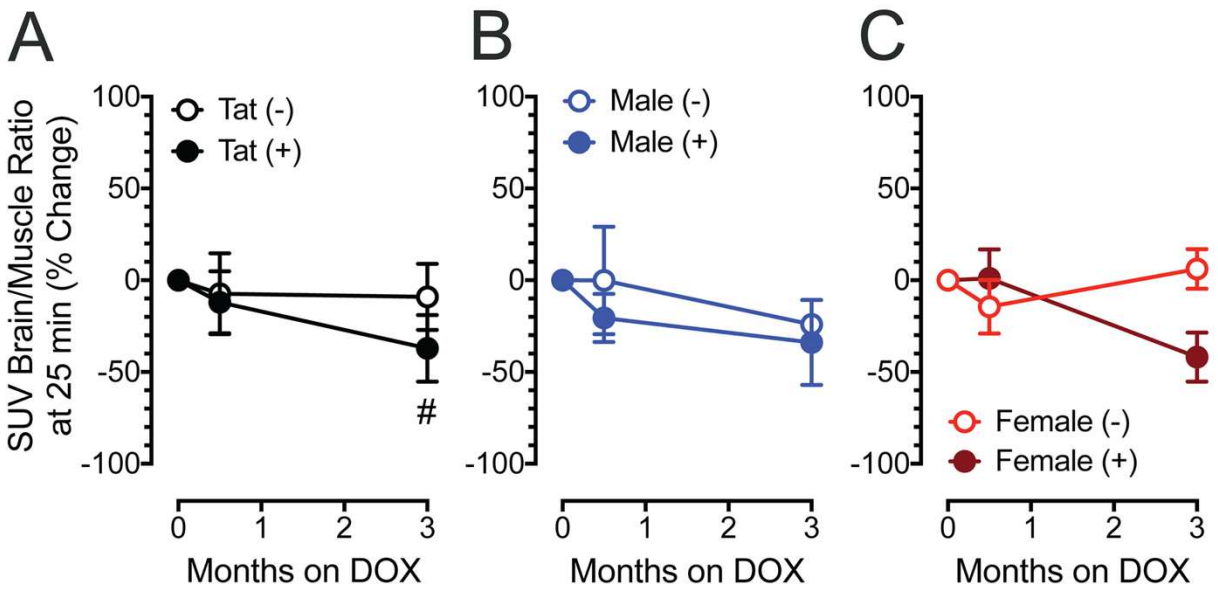

Figure 5. SUV for brain/muscle ratio normalized to baseline (% change) at 25 minutes. **(A)** SUV brain/muscle ratio of [^{11}C]-UCB-J uptake is represented over the three PET imaging sessions separate for Tat(−) and Tat(+) mice (n = 5-6 per group). A significant time x genotype interaction demonstrates a downregulation of SUV brain/muscle ratio over time for Tat(+) mice but not for Tat(−) mice. No other effect and/or interaction was significant, indicating that sex does not alter the SUV brain/muscle ratio at the static 25 minute time point. **(B)** SUV brain/muscle ratio of [^{11}C]-UCB-J uptake is represented over the three PET imaging sessions separate for males only (n = 3 per group). No significant effect for genotype and/or time was noted. **(C)** SUV brain/muscle ratio of [^{11}C]-UCB-J uptake is represented over the three PET imaging sessions separate for females only (n = 2-3 per group). No significant effect for genotype and/or time was noted. All data are presented as mean ± SD. $^{\#}p = 0.031$ Tat(+) at baseline no DOX (S1) vs. Tat(+) at 3 months DOX (S3). min: minutes.

Figure 6. SUV brain/muscle ratio normalized to baseline (% change) and averaged across the static 17.5 and 25 minute time points

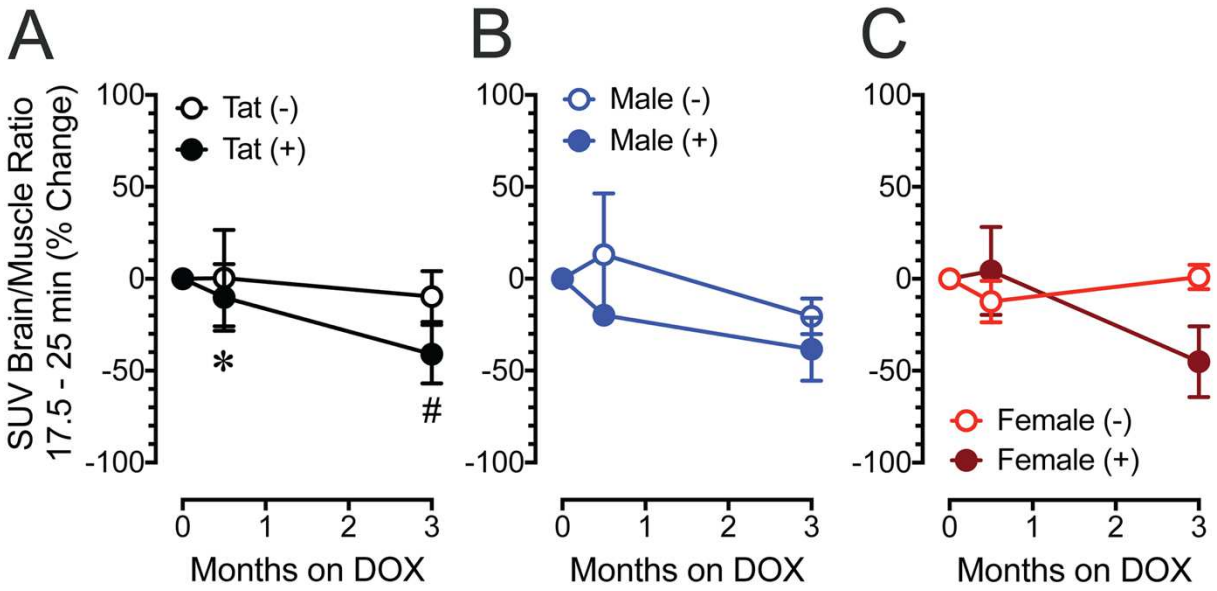

Figure 6. SUV for brain/muscle ratio normalized to baseline (% change) averaged across 17.5 and 25 minutes. **(A)** SUV brain/muscle ratio of [^{11}C]-UCB-J uptake is represented over the three PET imaging sessions separate for Tat(−) and Tat(+) mice (n = 5-6 per group). A significant time x genotype interaction demonstrates a downregulation of SUV brain/muscle ratio over time for Tat(+) mice but not for Tat(−) mice. No other effect and/or interaction was significant, indicating that sex does not alter the SUV brain/muscle ratio at 17.5 – 25 minutes. **(B)** SUV brain/muscle ratio of [^{11}C]-UCB-J uptake is represented over the three PET imaging sessions separate for males only (n = 3 per group). No significant effect for genotype and/or time was noted. **(C)** SUV brain/muscle ratio of [^{11}C]-UCB-J uptake is represented over the three PET imaging sessions separate for females only (n = 2-3 per group). No significant effect for genotype and/or time was noted. All data are presented as mean ± SD. $^{\#}p$ = 0.024 Tat(+) at baseline no DOX (S1) vs. Tat(+) at 3 months DOX (S3); $*p$ = 0.050 Tat(+) at 2 weeks DOX (S2) vs. Tat(+) at 3 months DOX (S3). min: minutes.

REFERENCES

1 Harrison, K. M., Song, R. & Zhang, X. Life expectancy after HIV diagnosis based on national HIV surveillance data from 25 states, United States. *J Acquir Immune Defic Syndr* **53**, 124-130, doi:10.1097/QAI.0b013e3181b563e7 (2010).

2 Saylor, D. *et al.* HIV-associated neurocognitive disorder - pathogenesis and prospects for treatment. *Nat Rev Neurol* **12**, 234-248, doi:10.1038/nrneurol.2016.27 (2016).

3 Ellis, R., Langford, D. & Masliah, E. HIV and antiretroviral therapy in the brain: neuronal injury and repair. *Nat Rev Neurosci* **8**, 33-44, doi:10.1038/nrn2040 (2007).

4 Antinori, A. *et al.* Updated research nosology for HIV-associated neurocognitive disorders. *Neurology* **69**, 1789-1799, doi:10.1212/01.WNL.0000287431.88658.8b (2007).

5 Heaton, R. K. *et al.* HIV-associated neurocognitive disorders before and during the era of combination antiretroviral therapy: differences in rates, nature, and predictors. *J Neurovirol* **17**, 3-16, doi:10.1007/s13365-010-0006-1 (2011).

6 Sacktor, N. *et al.* HIV-associated cognitive impairment before and after the advent of combination therapy. *J Neurovirol* **8**, 136-142, doi:10.1080/13550280290049615 (2002).

7 Dore, G. J. *et al.* Changes to AIDS dementia complex in the era of highly active antiretroviral therapy. *AIDS* **13**, 1249-1253 (1999).

8 Bonifant, C. L., Jackson, H. J., Brentjens, R. J. & Curran, K. J. Toxicity and management in CAR T-cell therapy. *Mol Ther Oncolytics* **3**, 16011, doi:10.1038/mto.2016.11 (2016).

9 Underwood, J. *et al.* Gray and White Matter Abnormalities in Treated Human Immunodeficiency Virus Disease and Their Relationship to Cognitive Function. *Clin Infect Dis* **65**, 422-432, doi:10.1093/cid/cix301 (2017).

10 Ru, W. & Tang, S. J. HIV-associated synaptic degeneration. *Molecular brain* **10**, 40, doi:10.1186/s13041-017-0321-z (2017).

11 Johnson, T. P. *et al.* Induction of IL-17 and nonclassical T-cell activation by HIV-Tat protein. *Proc Natl Acad Sci U S A* **110**, 13588-13593, doi:10.1073/pnas.1308673110 (2013).

12 Mediouni, S. *et al.* Antiretroviral therapy does not block the secretion of the human immunodeficiency virus tat protein. *Infect Disord Drug Targets* **12**, 81-86 (2012).

13 Jones, M. V., Bell, J. E. & Nath, A. Immunolocalization of HIV envelope gp120 in HIV encephalitis with dementia. *AIDS* **14**, 2709-2713 (2000).

14 Valle, L. D. *et al.* Detection of HIV-1 Tat and JCV capsid protein, VP1, in AIDS brain with progressive multifocal leukoencephalopathy. *Journal of Neurovirology* **6**, 221-228 (2000).

15 Kruman, II, Nath, A. & Mattson, M. P. HIV-1 protein Tat induces apoptosis of hippocampal neurons by a mechanism involving caspase activation, calcium overload, and oxidative stress. *Exp Neurol* **154**, 276-288, doi:10.1006/exnr.1998.6958 (1998).

16 Haughey, N. J., Nath, A., Mattson, M. P., Slevin, J. T. & Geiger, J. D. HIV-1 Tat through phosphorylation of NMDA receptors potentiates glutamate excitotoxicity. *J Neurochem* **78**, 457-467 (2001).

17 Bertrand, S. J., Mactutus, C. F., Aksenova, M. V., Espensen-Sturges, T. D. & Booze, R. M. Synaptodendritic recovery following HIV Tat exposure: neurorestoration by phytoestrogens. *J Neurochem* **128**, 140-151, doi:10.1111/jnc.12375 (2014).

18 Fitting, S. *et al.* Interactive HIV-1 Tat and morphine-induced synaptodendritic injury is triggered through focal disruptions in Na^+ influx, mitochondrial instability, and Ca^{2+} overload. *J Neurosci* **34**, 12850-12864, doi:10.1523/JNEUROSCI.5351-13.2014 (2014).

19 Fitting, S. *et al.* Synaptic dysfunction in the hippocampus accompanies learning and memory deficits in human immunodeficiency virus type-1 Tat transgenic mice. *Biol Psychiatry* **73**, 443-453, doi:10.1016/j.biopsych.2012.09.026 (2013).

20 Fitting, S. *et al.* Interactive comorbidity between opioid drug abuse and HIV-1 Tat: chronic exposure augments spine loss and sublethal dendritic pathology in striatal neurons. *Am J Pathol* **177**, 1397-1410, doi:10.2353/ajpath.2010.090945 (2010).

21 Carey, A. N., Sypek, E. I., Singh, H. D., Kaufman, M. J. & McLaughlin, J. P. Expression of HIV-Tat protein is associated with learning and memory deficits in the mouse. *Behav Brain Res* **229**, 48-56, doi:10.1016/j.bbr.2011.12.019 (2012).

22 Paris, J. J., Singh, H. D., Carey, A. N. & McLaughlin, J. P. Exposure to HIV-1 Tat in brain impairs sensorimotor gating and activates microglia in limbic and extralimbic brain regions of male mice. *Behav Brain Res* **291**, 209-218, doi:10.1016/j.bbr.2015.05.021 (2015).

23 Hahn, Y. K. *et al.* Effects of chronic HIV-1 Tat exposure in the CNS: heightened vulnerability of males versus females to changes in cell numbers, synaptic integrity, and behavior. *Brain Struct Funct* **220**, 605-623, doi:10.1007/s00429-013-0676-6 (2013).

24 Longordo, F. *et al.* The human immunodeficiency virus-1 protein transactivator of transcription up-regulates N-methyl-D-aspartate receptor function by acting at metabotropic glutamate receptor 1 receptors coexisting on human and rat brain noradrenergic neurones. *J Pharmacol Exp Ther* **317**, 1097-1105, doi:10.1124/jpet.105.099630 (2006).

25 Mattson, M. P., Haughey, N. J. & Nath, A. Cell death in HIV dementia. *Cell Death Differ* **12 Suppl 1**, 893-904, doi:10.1038/sj.cdd.4401577 (2005).

26 Haughey, N. J., Holden, C. P., Nath, A. & Geiger, J. D. Involvement of inositol 1,4,5-trisphosphate-regulated stores of intracellular calcium in calcium dysregulation and neuron cell death caused by HIV-1 protein tat. *J Neurochem* **73**, 1363-1374 (1999).

27 Bagashev, A. & Sawaya, B. E. Roles and functions of HIV-1 Tat protein in the CNS: an overview. *Virology journal* **10**, 358, doi:10.1186/1743-422X-10-358 (2013).

28 Dickens, A. M. *et al.* Chronic low-level expression of HIV-1 Tat promotes a neurodegenerative phenotype with aging. *Scientific reports* **7**, 7748, doi:10.1038/s41598-017-07570-5 (2017).

29 Nabulsi, N. B. *et al.* Synthesis and Preclinical Evaluation of 11C-UCB-J as a PET Tracer for Imaging the Synaptic Vesicle Glycoprotein 2A in the Brain. *Journal of nuclear medicine : official publication, Society of Nuclear Medicine* **57**, 777-784, doi:10.2967/jnumed.115.168179 (2016).

30 Madeo, M., Kovacs, A. D. & Pearce, D. A. The human synaptic vesicle protein, SV2A, functions as a galactose transporter in Saccharomyces cerevisiae. *J Biol Chem* **289**, 33066-33071, doi:10.1074/jbc.C114.584516 (2014).

31 Tokudome, K. *et al.* Synaptic vesicle glycoprotein 2A (SV2A) regulates kindling epileptogenesis via GABAergic neurotransmission. *Scientific reports* **6**, 27420, doi:10.1038/srep27420 (2016).

32 Crowder, K. M. *et al.* Abnormal neurotransmission in mice lacking synaptic vesicle protein 2A (SV2A). *Proc Natl Acad Sci U S A* **96**, 15268-15273, doi:10.1073/pnas.96.26.15268 (1999).

33 Bertoglio, D. *et al.* Validation and noninvasive kinetic modeling of [(11)C]UCB-J PET imaging in mice. *J Cereb Blood Flow Metab*, 271678X19864081, doi:10.1177/0271678X19864081 (2019).

34 Toyonaga, T. *et al.* In Vivo Synaptic Density Imaging with (11)C-UCB-J Detects Treatment Effects of Saracatinib in a Mouse Model of Alzheimer Disease. *Journal of nuclear medicine : official publication, Society of Nuclear Medicine* **60**, 1780-1786, doi:10.2967/jnumed.118.223867 (2019).

35 Loscher, W., Gillard, M., Sands, Z. A., Kaminski, R. M. & Klitgaard, H. Synaptic Vesicle Glycoprotein 2A Ligands in the Treatment of Epilepsy and Beyond. *CNS Drugs* **30**, 1055-1077, doi:10.1007/s40263-016-0384-x (2016).

36 Cai, Z., Li, S., Matuskey, D., Nabulsi, N. & Huang, Y. PET imaging of synaptic density: A new tool for investigation of neuropsychiatric diseases. *Neurosci Lett* **691**, 44-50, doi:10.1016/j.neulet.2018.07.038 (2019).

37 Yao, J., Nowack, A., Kensel-Hammes, P., Gardner, R. G. & Bajjalieh, S. M. Cotrafficking of SV2 and synaptotagmin at the synapse. *J Neurosci* **30**, 5569-5578, doi:10.1523/JNEUROSCI.4781-09.2010 (2010).

38 Gillard, M., Chatelain, P. & Fuks, B. Binding characteristics of levetiracetam to synaptic vesicle protein 2A (SV2A) in human brain and in CHO cells expressing the human recombinant protein. *Eur J Pharmacol* **536**, 102-108, doi:10.1016/j.ejphar.2006.02.022 (2006).

39 Robinson, J. L. *et al.* Perforant path synaptic loss correlates with cognitive impairment and Alzheimer's disease in the oldest-old. *Brain* **137**, 2578-2587, doi:10.1093/brain/awu190 (2014).

40 Finnema, S. J. *et al.* Imaging synaptic density in the living human brain. *Sci Transl Med* **8**, 348ra396, doi:10.1126/scitranslmed.aaf6667 (2016).

41 Hauser, K. F. *et al.* HIV-1 Tat and Morphine Have Interactive Effects on Oligodendrocyte Survival and Morphology. *Glia* **57**, 194-206, doi:10.1002/glia.20746 (2009).

42 Bruce-Keller, A. J. *et al.* Morphine causes rapid increases in glial activation and neuronal injury in the striatum of inducible HIV-1 Tat transgenic mice. *Glia* **56**, 1414-1427, doi:10.1002/glia.20708 (2008).

43 Paris, J. J., Singh, H. D., Ganno, M. L., Jackson, P. & McLaughlin, J. P. Anxiety-like behavior of mice produced by conditional central expression of the HIV-1 regulatory protein, Tat. *Psychopharmacology (Berl)* **231**, 2349-2360, doi:10.1007/s00213-013-3385-1 (2014).

44 Paris, J. J. *et al.* Effects of conditional central expression of HIV-1 tat protein to potentiate cocaine-mediated psychostimulation and reward among male mice. *Neuropsychopharmacology* **39**, 380-388, doi:10.1038/npp.2013.201 (2014).

45 Mediouni, S. *et al.* Didehydro-cortistatin A inhibits HIV-1 Tat mediated neuroinflammation and prevents potentiation of cocaine reward in Tat transgenic mice. *Curr HIV Res* **13**, 64-79 (2015).

46 El-Hage, N., Bruce-Keller, A. J., Knapp, P. E. & Hauser, K. F. CCL5/RANTES gene deletion attenuates opioid-induced increases in glial CCL2/MCP-1 immunoreactivity and activation in HIV-1 Tat-exposed mice. *J Neuroimmune Pharmacol* **3**, 275-285, doi:10.1007/s11481-008-9127-1 (2008).

47 Green, M. V., Ostrow, H. G., Seidel, J. & Pomper, M. G. Experimental evaluation of depth-of-interaction correction in a small-animal positron emission tomography scanner. *Molecular imaging* **9**, 311-318 (2010).

48 Gendelman, H. E., Lipton, S. A., Tardieu, M., Bukrinsky, M. I. & Nottet, H. S. The neuropathogenesis of HIV-1 infection. *J Leukoc Biol* **56**, 389-398, doi:10.1002/jlb.56.3.389 (1994).

49 Fields, J. A. *et al.* Mechanisms of HIV-1 Tat neurotoxicity via CDK5 translocation and hyper-activation: role in HIV-associated neurocognitive disorders. *Curr HIV Res* **13**, 43-54, doi:10.2174/1570162x13666150311164201 (2015).

50 Wallet, C. *et al.* Microglial Cells: The Main HIV-1 Reservoir in the Brain. *Front Cell Infect Microbiol* **9**, 362, doi:10.3389/fcimb.2019.00362 (2019).

51 Seelamgari, A. *et al.* Role of viral regulatory and accessory proteins in HIV-1 replication. *Front Biosci* **9**, 2388-2413, doi:10.2741/1403 (2004).

52 Ko, A. *et al.* Macrophages but not Astrocytes Harbor HIV DNA in the Brains of HIV-1-Infected Aviremic Individuals on Suppressive Antiretroviral Therapy. *J Neuroimmune Pharmacol* **14**, 110-119, doi:10.1007/s11481-018-9809-2 (2019).

53 Sami Saribas, A. *et al.* HIV-1 Nef is released in extracellular vesicles derived from astrocytes: evidence for Nef-mediated neurotoxicity. *Cell Death Dis* **8**, e2542, doi:10.1038/cddis.2016.467 (2017).

54 Santosuosso, M., Righi, E., Lindstrom, V., Leblanc, P. R. & Poznansky, M. C. HIV-1 envelope protein gp120 is present at high concentrations in secondary lymphoid organs of individuals with chronic HIV-1 infection. *J Infect Dis* **200**, 1050-1053, doi:10.1086/605695 (2009).

55 Louboutin, J. P. & Strayer, D. S. Blood-brain barrier abnormalities caused by HIV-1 gp120: mechanistic and therapeutic implications. *ScientificWorldJournal* **2012**, 482575, doi:10.1100/2012/482575 (2012).

56 Zhou BY, Liu Y, Kim Bo, Xiao Y, He JJ. Astrocyte activation and dysfunction and neuron death by HIV-1 Tat expression in astrocytes. Mol Cell Neurosci. 2004;27(3):296–305. doi:10.1016/j.mcn.2004.07.003

57 Fan Y, He JJ. HIV-1 Tat Promotes Lysosomal Exocytosis in Astrocytes and Contributes to Astrocyte-mediated Tat Neurotoxicity. J Biol Chem. 2016;291(43):22830–22840. doi:10.1074/jbc.M116.731836

58 Veronica Musante, Maria Summa, Elisa Neri, Aldamaria Puliti, Tomasz T. Godowicz, Paolo Severi, Giuseppe Battaglia, Maurizio Raiteri, Anna Pittaluga, The HIV-1 Viral Protein Tat Increases Glutamate and Decreases GABA Exocytosis from Human and Mouse Neocortical Nerve Endings, Cerebral Cortex, 2010;20(8):1974–1984

59 Fields J, Dumaop W, Eleuteri S, et al. HIV-1 Tat alters neuronal autophagy by modulating autophagosome fusion to the lysosome: implications for HIV-associated neurocognitive disorders. J Neurosci. 2015;35(5):1921–1938. doi:10.1523/JNEUROSCI.3207-14.2015

60 Tryoen-Tóth P, Chasserot-Golaz S, Tu A, et al. HIV-1 Tat protein inhibits neurosecretion by binding to phosphatidylinositol 4,5-bisphosphate. J Cell Sci. 2013;126(Pt 2):454–463. doi:10.1242/jcs.111658

61 Eletto D, Russo G, Passiatore G, et al. Inhibition of SNAP25 expression by HIV-1 Tat involves the activity of mir-128a. J Cell Physiol. 2008;216(3):764–770. doi:10.1002/jcp.21452